

# Spatial Degrees of Freedom in Near Field MIMO: Experimental Validation of BeamSpace Perspective

Ahmed Hussain, Asmaa Abdallah, *Senior Member, IEEE*, Ahmed Nasser, *Senior Member, IEEE*,  
Abdulkadir Celik, *Senior Member, IEEE*, and Ahmed M. Eltawil, *Senior Member, IEEE*

**Abstract**—Conventional far-field multiple-input multiple-output (MIMO) channels are limited to a single spatial degree of freedom (DoF) under a line-of-sight (LoS) condition. In contrast, the radiative near field (NF) supports multiple spatial DoF, enabled by spherical wavefronts and the reduced spatial footprint at short ranges. While recent research indicates that the effective DoF (EDoF) increases in NF, experimental validation and clear identification of the transition distances remain limited. In this letter, we develop an intuitive framework for characterizing the EDoF of a ULA-based MIMO system and derive two complementary analytical expressions: a closed-form formulation that relates the EDoF to the physical transmit beamwidth and receive aperture, and a discrete formulation based on the discrete Fourier transform (DFT) domain angular decomposition of the NF spherical wavefront, which is well suited for experimental evaluation. We further introduce the effective MIMO Rayleigh distance (EMRD) and the maximum spatial multiplexing distance (MSMD), which mark the distances where the EDoF reduces to one and attains its maximum, respectively. Experimental measurements using widely spaced phased arrays closely match the theoretical EDoF trends and validate the proposed distance metrics.

**Index Terms**—Near field, spatial degrees of freedom, MIMO, DFT, and effective MIMO Rayleigh distance.

## I. INTRODUCTION

**F**UTURE wireless networks employing large antenna arrays at high frequencies are expected to operate in the radiative near-field (NF), where spherical wavefronts enhance both single-user and multi-user capacity [1]. In the NF, the finite beamdepth enables spatial separation of user equipments (UEs) along the range dimension, thereby improving multiuser capacity [2]. In the far-field (FF), a line-of-sight (LoS) multiple-input multiple-output (MIMO) channel is typically rank one, supporting only a single data stream. In contrast, the radiative NF, with its inherent spherical wavefronts, offers enriched spatial degrees of freedom (DoF) [3], enabling multiple data streams even in LoS case.

Spatial DoF represent the parallel communication modes determined by the propagation environment and array geometry [4]. While the array geometry imposes an upper bound on the achievable DoF, the usable DoF are limited by the minimum of the transmit and receive antenna counts. The spatial DoF also vary with the angular extent of the radiated

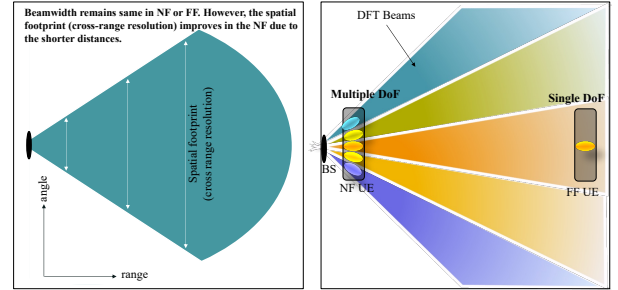


Fig. 1: Multiple EDoF in NF communication.

field, set by the transmit beamwidth, and the physical size of the receiving aperture. Although the angular beamwidth is invariant with distance, the *spatial footprint* expands linearly with range as shown in Fig. 1 (left). Consequently, capturing multiple angular beams in the FF requires prohibitively large receive apertures; for instance, spatial footprint corresponding to a beamwidth of  $3^\circ$  spans 0.52 m at a distance of 10 m, but expands to 52 m at 1 km. Furthermore, beamfocusing-based NF beams inherently comprise multiple angular components due to the spherical wavefront being a superposition of plane waves [1]. As illustrated in Fig. 1 (right), the reduced spatial footprint and inherent curvature of spherical wavefronts in the NF may potentially unlock higher spatial DoF.

The spatial DoF are quantified through the singular values of the MIMO channel, which typically exhibit a step-like distribution, indicating that the corresponding subchannels are not of equal quality [5]. Only the singular values exceeding a certain threshold effectively contribute to capacity, giving rise to the concept of effective degrees of freedom (EDoF). In the NF, higher EDoF can be achieved either by enlarging the aperture or by increasing the carrier frequency. The latter, however, introduces severe coverage limitations, whereas expanding the aperture requires a very large number of antennas, leading to prohibitive hardware and signal-processing complexity. Although theory suggests that the EDoF effectively reduces to one in the FF and increases in the NF [4], experimental validation remains limited. Moreover, the exact distance at which the EDoF first exceeds one, and the distance at which it reaches its maximum, has not been clearly established.

To address these gaps, we develop an intuitive framework for characterizing the EDoF and validate it through experimental measurements. Specifically, we derive two complementary analytical expressions for the EDoF in uniform linear array (ULA)-based MIMO systems. The first is a closed-form expression that relates the EDoF to the physical transmit beamwidth and receive aperture, providing insight into its distance-dependent

Ahmed Hussain, Asmaa Abdallah, Ahmed Nasser, and Ahmed M. Eltawil are with the Computer, Electrical, and Mathematical Sciences and Engineering (CEMSE) Division, King Abdullah University of Science and Technology (KAUST), Thuwal 23955-6900, Saudi Arabia. Abdulkadir Celik is with School of Electronics and Computer Science, University of Southampton, SO17 1BJ UK.

behavior. The second is a discrete formulation based on discrete Fourier transform (DFT), which captures the angular decomposition of the spherical wavefront. We further introduce the effective MIMO Rayleigh distance (EMRD), defined as the distance at which the EDoF reduces to one, and the maximum spatial multiplexing distance (MSMD), which denotes the distance at which the maximum EDoF is attained. Experimental measurements closely follow the theoretical analysis and validate the proposed distance metrics.

## II. SYSTEM MODEL

We consider a point-to-point LoS MIMO system, as illustrated in Fig. 2. The base station (BS) and UE are equipped with ULAs comprising  $M$  transmit and  $N$  receive antennas, respectively. The inter-element spacing is set to  $d = \lambda/2$ , yielding approximate aperture lengths of  $D_t \approx Md$  at the BS and  $D_r \approx Nd$  at the UE. The UE is located at a distance  $r$  from the BS. The ULAs at the BS and UE are oriented at angles  $\varphi_t$  and  $\varphi_r$ , respectively, with respect to their local coordinate systems. The channel coefficient of the MIMO channel  $\mathbf{H} \in \mathbb{C}^{M \times N}$  between the  $m^{\text{th}}$  transmit and  $n^{\text{th}}$  receive antenna elements is given by

$$h_{m,n} = \sqrt{g_{m,n}} e^{-j \frac{2\pi}{\lambda} (r_{m,n} - r)}, \quad (1)$$

where  $g_{m,n} = \frac{\lambda^2}{(4\pi)^2 (r_{m,n})^2}$ , denotes the free-space pathloss and  $r_{m,n}$  denote the distance between the  $m^{\text{th}}$  transmit and  $n^{\text{th}}$  receive elements, approximated as

$$r_{m,n} = \sqrt{(r + md \sin \varphi_t - nd \sin \varphi_r)^2 + (md \cos \varphi_t - nd \cos \varphi_r)^2}, \\ \approx r + md \sin \varphi_t - nd \sin \varphi_r + \frac{(md \cos \varphi_t - nd \cos \varphi_r)^2}{2r}. \quad (2)$$

Given a MIMO channel  $\mathbf{H} \in \mathbb{C}^{M \times N}$ , the spatial DoF represent the number of independent sub-channels that support parallel transmission modes. Mathematically, this corresponds to the number of non-zero singular values obtained from the singular value decomposition (SVD) of  $\mathbf{H}$ , or equivalently, the rank of the Gramian matrix  $\mathbf{R} = \mathbf{H}^H \mathbf{H}$ . While the channel rank determines the potential number of parallel streams, the actual channel capacity also depends on the distribution of eigenvalues. Hence, the EDoF is often used to quantify the number of effective parallel channels at high signal-to-noise ratio (SNR). The eigenvalues  $\mu_i$  exhibit step-like behavior, remaining approximately equal up to a certain index EDoF, beyond which they decay sharply to zero. Assuming EDoF equal eigenvalues ( $\mu_1 = \mu_2 = \dots = \mu_{\text{EDoF}} = \mu$ ), the sum of all eigenvalues equals the trace of the Gramian  $\sum_{i=1}^{\min(M,N)} \mu_i = \text{tr}(\mathbf{H}\mathbf{H}^H) = MN$ . Thus, with only EDoF non-zero eigenvalues, we have

$$\text{EDoF} \mu = MN \Rightarrow \mu = \frac{MN}{\text{EDoF}}. \quad (3)$$

Diagonalizing  $\mathbf{H}$  yields EDoF parallel channels, each with an equal gain  $\mu$ . With equal eigenvalues, the optimal power allocation is uniform, i.e.,  $P_i = P/\text{EDoF}$ , leading to the single-user capacity expression as

$$C = \sum_{i=1}^{\text{EDoF}} \log_2 \left( 1 + \frac{P_i \mu}{\sigma^2} \right) = \text{EDoF} \log_2 \left( 1 + \frac{P \mu}{\text{EDoF} \sigma^2} \right), \quad (4)$$

$$C = \text{EDoF} \log_2 \left( 1 + \frac{\rho}{\text{EDoF}^2} \right), \quad \rho = \frac{PMN}{\sigma^2}, \quad (5)$$

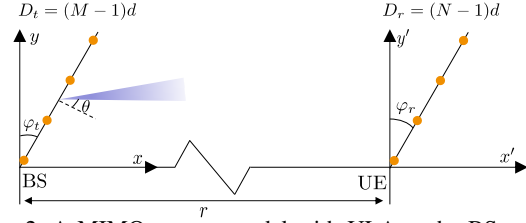


Fig. 2: A MIMO system model with ULA at the BS and UE.

The final simplified form is obtained by substituting  $\mu$  from (3), and  $\sigma^2$  denotes the noise power. At high SNR, the capacity scales approximately as  $C \approx \text{EDoF} \log_2(\rho/\text{EDoF}^2)$ , increasing almost linearly with EDoF.

## III. EFFECTIVE SPATIAL DEGREES OF FREEDOM

As illustrated in Fig. 1, the reduced spatial footprint and the spherical wavefronts in the NF enable higher spatial DoF. In this section, we derive two complementary analytical expressions for the EDoF. The first is a closed-form expression based on the physical beamwidth, which varies continuously with distance and provides theoretical insight into the spatial scaling behavior. The second is based on an angular decomposition of the spherical wavefront, leading to a discrete formulation that is more suitable for experimental evaluation.

### A. Electromagnetic Perspective

The spatial DoF denote the number of linearly independent columns in the channel matrix  $\mathbf{H}$ , whereas the EDoF represent the subset of mutually orthogonal columns. From an electromagnetic standpoint, the EDoF represents the number of transmit beams that remain distinguishable at the receiver. It can be approximated as the ratio between the receive aperture length  $D_r$  and the spatial footprint of the transmit beam [5]. This ratio indicates how many transmit beams illuminate the receiver aperture with minimal mutual interference. The spatial footprint referred to as the cross-range resolution  $\Delta_{\text{CR}}$  is determined by the transmit beamwidth  $\theta_{3\text{dB}}$ . For a ULA with transmit aperture  $D_t$ , the cross-range resolution and beamwidth are

$$\Delta_{\text{CR}} = r \theta_{3\text{dB}} \quad \text{and} \quad \theta_{3\text{dB}} \approx \frac{\lambda}{D_t \cos \varphi_t}, \quad (6)$$

respectively, leading to the following closed-form expression for the EDoF:

$$\text{EDoF}_1 \approx \frac{D_r \cos \varphi_r}{\Delta_{\text{CR}}} = \frac{D_r D_t}{\lambda r} \cos \varphi_t \cos \varphi_r. \quad (7)$$

Although the angular beamwidth  $\theta_{3\text{dB}}$  remains invariant across the NF and FF, the cross-range resolution  $\Delta_{\text{CR}}$  improves as the transmitter–receiver separation  $r$  decreases. As a result, the NF yields a higher EDoF due to its finer cross-range discrimination.

Beyond the reduced spatial footprint, spherical wave propagation further enhances the EDoF. Unlike planar wavefronts, which induce a linear phase profile across the array and support a single dominant spatial mode, spherical wavefronts introduce phase curvature across the aperture, thereby exciting multiple orthogonal spatial modes. In the following section, we present a DFT-based decomposition of NF beams to analyze the resulting EDoF.

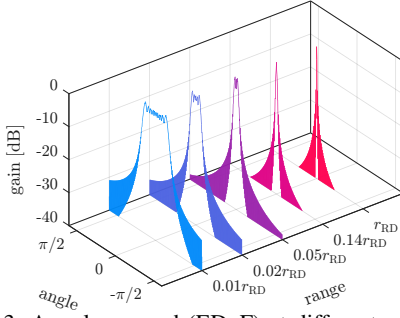


Fig. 3: Angular spread (EDoF) at different ranges.

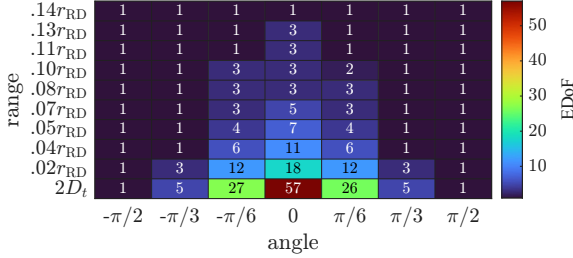


Fig. 4: EDoF for the transmitter at different ranges and angles. We set  $M = 256$ ,  $f_c = 29$  GHz,  $D_t = 1.3$  m,  $r_{RD} = 336$  m.

### B. Representation of NF Signal Using DFT Beams

A BS equipped with  $M$  antennas can transmit up to  $M$  spatially orthogonal beams, each associated with a discrete angular direction  $\sin(\theta_m) \in [-1, 1]$ , represented by the columns of a DFT codebook. For a FF UE, the correlation  $\mathbf{a}^H(\theta)\mathbf{a}(\theta_m)$  is maximized only when the user's direction  $\theta$  matches  $\theta_m$ , and ideally becomes negligible for all  $\theta_m \neq \theta$ . In the NF, however, a UE exhibits non-negligible correlation with multiple adjacent DFT beams, revealing the presence of additional spatial DoF. This behavior arises because far-field propagation is governed by planar wavefronts, whereas near-field propagation results in spherical wavefronts that can be expressed as a superposition of multiple angular (planar) components. Motivated by this observation, we model a NF beam as a weighted combination of DFT beams. The number of DFT beams with high gain reflects the available spatial DoF.

The EDoF of a MIMO system may also be interpreted as the number of transmit beams that can be uniquely mapped to distinct receive beams. The number of such unique pairs is upper bounded by the smaller of the numbers of transmit and receive beams. In principle, one could decompose the beams at both the transmitter and receiver to explicitly count these unique beam pairs. However, identifying the number of unique pairs is a complex task. To simplify the analysis, we project only the transmit-side NF channel onto the angular domain using the DFT. The number of DFT beams exhibiting high gain in this domain provides an estimate of the transmit-side EDoF. The overall MIMO EDoF is then computed by scaling this transmit-side estimate with the effective aperture length  $D_r$  at the receiver.

We consider a NF transmit beam focused at the location  $(\theta, r)$ . The NF array response vector approximated based on

Fresnel approximation is [2]

$$\mathbf{b}_m(\theta, r) \approx \frac{1}{\sqrt{M}} e^{-j\frac{2\pi}{\lambda} \left( md \sin(\theta) - \frac{m^2 d^2 \cos^2(\theta)}{2r} \right)}, \quad (8)$$

while the FF steering vector is obtained by omitting the quadratic phase term as

$$\mathbf{a}_m(\theta) \approx \frac{1}{\sqrt{M}} e^{-j\frac{2\pi}{\lambda} md \sin(\theta)}. \quad (9)$$

In the following, we derive the DFT coefficients corresponding to the transmit-side NF array response vector in (8). The resulting gain  $\mathcal{G}$  observed at the NF UE from each DFT beam directed toward  $\theta_m$  is expressed as

$$\begin{aligned} \mathcal{G}(\theta, r; \theta_m) &= \left| \mathbf{b}^H(\theta, r) \mathbf{a}(\theta_m) \right|^2, \quad \sin(\theta_m) \in [-1, 1] \\ &\approx \frac{1}{M^2} \left| \sum_{-M/2}^{M/2} e^{j\frac{2\pi}{\lambda} \left\{ md \sin(\theta) - \frac{1}{2r} m^2 d^2 \cos^2(\theta) \right\} - j\frac{2\pi m d \sin \theta_m}{\lambda}} \right|^2, \\ &\stackrel{(c_1)}{=} \frac{1}{M^2} \left| \sum_{-M/2}^M e^{-j\pi \left\{ m^2 \left( \frac{d \cos^2 \theta}{2r} \right) - m(\sin \theta - \sin \theta_m) \right\}} \right|^2, \end{aligned} \quad (10)$$

where  $(c_1)$  is simplified assuming  $d = \lambda/2$ . We further simplify the array gain function in (10) in terms of Fresnel functions  $\mathcal{C}(\cdot)$  and  $\mathcal{S}(\cdot)$ , whose arguments depend on the UE location  $(\theta, r)$  and DFT beam angle  $\theta_m$ . Accordingly, the gain function observed at the NF UE under illumination from orthogonal DFT beams can be approximated as [6]

$$\mathcal{G}(\theta, r; \theta_m) \approx \left| \frac{\bar{\mathcal{C}}(\gamma_1, \gamma_2) + j\bar{\mathcal{S}}(\gamma_1, \gamma_2)}{2\gamma_2} \right|^2, \quad (11)$$

$\bar{\mathcal{C}}(\gamma_1, \gamma_2) \equiv \mathcal{C}(\gamma_1 + \gamma_2) - \mathcal{C}(\gamma_1 - \gamma_2)$  and  $\bar{\mathcal{S}}(\gamma_1, \gamma_2) \equiv \mathcal{S}(\gamma_1 + \gamma_2) - \mathcal{S}(\gamma_1 - \gamma_2)$ , where  $\gamma_1 = \sqrt{\frac{r}{d \cos^2 \theta}} (\sin \theta_m - \sin \theta)$  and  $\gamma_2 = \frac{M}{2} \sqrt{\frac{d \cos^2 \theta}{r}}$ . To characterize the EDoF, we adopt the 3 dB threshold criterion. We count the angular directions  $\theta_m$  with the normalized gain above 0.5 and term it as the EDoF for the transmitter given by

$$\text{EDoF}_2(\theta, r) = \sum_m \mathbf{1} \left\{ \mathcal{G}(\theta, r; \theta_m) \geq \frac{1}{2} \right\}. \quad (12)$$

where  $\mathbf{1}(\cdot)$  denotes the indicator function. We use the above expression to evaluate the EDoF in our measurements.

To gain further insight, we plot the gain in (11) across different ranges, as illustrated in Fig. 3. At the Rayleigh distance for multiple-input single-output (MISO) given by  $r_{RD} = \frac{2D_t^2}{\lambda}$ , which represents the classical boundary between the NF and FF regions, (11) yields a single peak value for  $\mathcal{G}$ . In contrast, at shorter ranges, multiple peaks emerge around the UE angle forming an angular spread, indicating an increased EDoF. It is important to highlight that Fig. 3 can also be obtained by applying the FFT to the NF channel in (8) and plotting the resulting spectrum. Fig. 4 presents the EDoF computed via (12) at various range and angle values. The maximum EDoF is achieved at the boresight direction and at a range equal to  $2D_t$ , where it reaches a value of 57. This maximum EDoF is significantly smaller than the total number of antenna elements, which is  $M = 256$ . Moreover, the minimum EDoF of 1 is observed for  $r < \frac{r_{RD} \cos^2 \theta}{7}$  [2], which corresponds to the beam-focusing limit of a ULA. This limit is seven times smaller than the Rayleigh distance at boresight. Additionally, for a fixed range, the EDoF attains its maximum at boresight and



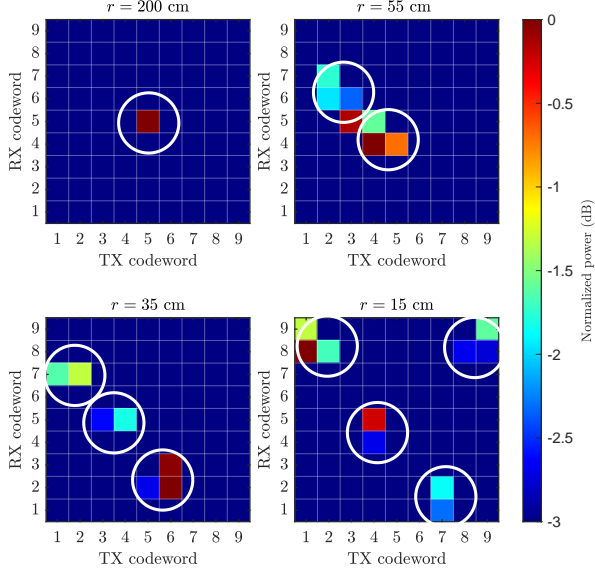


Fig. 6: Heatmap of the RSSI matrix for selected range values.

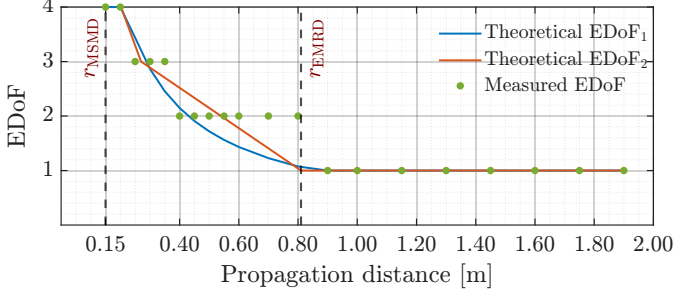


Fig. 7: Comparison of theoretical and experimental EDoF.

power values are then normalized and clipped to a 3 dB dynamic range, consistent with (12). At  $r = 200$  cm, a single dominant peak appears, indicating an EDoF of one. As the distance decreases, multiple peaks progressively emerge in the RSSI maps, revealing the onset of NF effects. For example, at  $r = 55$  cm, the Tx codewords span four bins (bins 2–5) and the Rx codewords span four bins (bins 4–7). Since the DFT codebook is oversampled by a factor of two, these peaks form two clear clusters, corresponding to an EDoF of two. At  $r = 35$  cm, three clusters are observed, while at  $r = 15$  cm, four clusters appear, yielding EDoFs of three and four, respectively. Furthermore, the inter-cluster separation increases as  $r$  decreases, indicating reduced overlap and stronger orthogonality. Based on these measurements, we design heuristic rules to estimate the EDoF directly from the raw RSSI matrices. Peak locations are first extracted using a 3 dB threshold. Clusters are then formed using two criteria: (i) peaks in the same row or column are grouped together, and (ii) peaks separated by only a single row or column are merged into one cluster. Each cluster is subsequently represented by the rounded centroid of its peak coordinates, and the EDoF is obtained as the number of resulting clusters.

We plot the resulting EDoF obtained from measurements as a function of distance in Fig. 7. These results are compared against the theoretical expressions derived in Section III. For the given aperture sizes  $D_t$  and  $D_r$ , the EMRD based on (14) is  $r_{\text{EMRD}} = \frac{D_t D_r}{\lambda} = \frac{0.30 \times 0.02}{0.0075} = 0.81$  m. Similarly, the MSMD

from (16) is  $r_{\text{MSMD}} = \frac{D_r}{2} = 0.15$  m. As shown in Fig. 7, the measured EDoF reaches its maximum value at  $r = 15$  cm, which agrees with the predicted  $r_{\text{MSMD}}$ . As the link distance increases, the EDoF decrease and eventually reduces to one as the distance approaches the  $r_{\text{EMRD}}$ .

Achieving practical EMRD values requires very large transmit and receive apertures, which can be costly in hardware. A feasible alternative is to deploy widely spaced subarrays at the BS, effectively enlarging the aperture. In our measurements, the distributed phased arrays emulate a large effective aperture while reducing hardware complexity. The results confirm that higher EDoF can be realized in LoS scenarios using such widely spaced subarrays.

## V. CONCLUSION

In this letter, we developed a framework to characterize the EDoF in ULA-based MIMO systems. Analytical expressions and experimental measurements using modular phased arrays demonstrate that the NF can support significantly higher EDoF compared to the FF. These results provide valuable insights for designing high-capacity, low-complexity MIMO systems in the radiative NF.

## REFERENCES

- [1] A. Hussain, A. Abdallah, A. Celik, and A. M. Eltawil, “Near-field ISAC: Synergy of dual-purpose codebooks and space-time adaptive processing,” *IEEE Wireless Commun.*, vol. 32, no. 4, pp. 64–70, 2025.
- [2] A. Abdallah, A. Hussain, A. Celik, and A. M. Eltawil, “Exploring frontiers of polar-domain codebooks for near-field channel estimation and beam training: A comprehensive analysis, case studies, and implications for 6G,” *IEEE Signal Process. Mag.*, vol. 42, no. 1, pp. 45–59, 2025.
- [3] C. Ouyang, Y. Liu, X. Zhang, and L. Hanzo, “Near-field communications: A degree-of-freedom perspective,” *arXiv preprint arXiv:2308.00362*, 2023.
- [4] A. Kosasih, Ö. T. Demir, N. Kolomvakis, and E. Björnson, “Spatial frequencies and degrees of freedom: Their roles in near-field communications,” *IEEE Sig. Process. Mag.*, vol. 42, no. 1, pp. 33–44, 2025.
- [5] A. Hussain, A. Abdallah, A. Celik, E. Björnson, and A. M. Eltawil, “Analyzing URA geometry for enhanced near-field beamfocusing and spatial degrees of freedom,” *Submitted to IEEE Trans. Commun.*, 2024. [Online]. Available: <https://repository.kaust.edu.sa/handle/10754/706379>
- [6] A. Hussain, A. Abdallah, A. Celik, and A. M. Eltawil, “Near-field beam prediction using far-field codebooks in ultra-massive MIMO systems,” in *Proc. IEEE Int. Conf. Commun. (ICC)*, 2025, pp. 1712–1717.
- [7] F. Bohagen, P. Orten, and G. Oien, “Construction and capacity analysis of high-rank line-of-sight MIMO channels,” in *Proc. IEEE Wireless Commun. and Net. Conf.*, vol. 1, 2005, pp. 432–437.

## APPENDIX

To derive the MSMD from the orthogonality condition of  $\mathbf{H}$ , we compute the inner product between the received vectors corresponding to two distinct transmit antennas, using the channel coefficients in (1), and enforce this inner product to be zero:

$$\begin{aligned}
 \langle \mathbf{h}_{k,n}, \mathbf{h}_{l,n} \rangle &= \sum_{n=0}^{N-1} \exp\left(j \frac{2\pi}{\lambda} (r_{k,n} - r_{l,n})\right) \\
 &= \sum_{n=0}^{N-1} \exp\left(j \frac{2\pi d^2 \cos \varphi_r \cos \varphi_t}{\lambda r} (k-l)n\right) \\
 &= \frac{\sin\left(\pi \frac{d^2}{\lambda r} \cos \theta_r \cos \varphi_t (k-l)N\right)}{\sin\left(\pi \frac{d^2}{\lambda r} \cos \varphi_r \cos \varphi_t (k-l)\right)} = 0, \\
 \Rightarrow r &= \frac{Nd^2}{\lambda} \cos \varphi_r \cos \varphi_t = \frac{D_r}{2} \cos \varphi_r \cos \varphi_t \quad (17)
 \end{aligned}$$